REPORT DOCUMENTATION PAGE

Form Approved
OMB No. 0704-0188

1. REPORT DATE *(DD-MM-YYYY)*
01/11/14

2. REPORT TYPE
Journal Article

3. DATES COVERED *(From - To)*
June 1, 2014-Nov 24, 2014

4. TITLE AND SUBTITLE

Measuring the contribution of atmospheric scatter to laser eye dazzle

5a. CONTRACT NUMBER
FA8650-14-D-6519

5b. GRANT NUMBER
NA

5c. PROGRAM ELEMENT NUMBER
0602202F

6. AUTHOR(S)

Craig A. Williamson, John M. Rickman, David A. Freeman, Michael A. Manka, and

5d. PROJECT NUMBER
7757

5e. TASK NUMBER
HD

5f. WORK UNIT NUMBER
03/HOBA

7. PERFORMING ORGANIZATION NAME(S) AND ADDRESS(ES)

Air Force Research Laboratory
711th Human Performance Wing
Human Effectiveness Directorate
Bioeffects Division
Optical Radiation Bioeffects Branch

TASC, Inc.
4141 Petroleum Rd
JBSA Fort Sam Houston TX

8. PERFORMING ORGANIZATION REPORT NUMBER

9. SPONSORING / MONITORING AGENCY NAME(S) AND ADDRESS(ES)
Air Force Research Laboratory
711th Human Performance Wing
Human Effectiveness Directorate
Bioeffects Division
Optical Radiation Bioeffects Branch
4141 Petroleum Rd
JBSA Fort Sam Houston TX

10. SPONSOR/MONITOR'S ACRONYM(S)

11. SPONSOR/MONITOR'S REPORT NUMBER(S)
AFRL-RH-FS-JA-2015-0003

12. DISTRIBUTION / AVAILABILITY STATEMENT
A: Approved for public release (PA); distribution unlimited. PA Case No: TSRL-PA-2015-0003 Date Cleared: Feb 11, 2015.

13. SUPPLEMENTARY NOTES

14. Abstract

An experiment has been conducted to determine the contribution of atmospheric scatter to the severity of the dazzle experienced by a human under illumination from a visible laser. A 15W532 nm laser was propagated over a 380 m outdoor range in San Antonio, Texas, over nine data collection sessions spanning June and July 2014. A narrow acceptance angle detector was used to measure scattered laser radiation within the laser beam at different angles from its axis. Atmospheric conditions were logged via a local weather station, and air quality data were taken from a nearby continuous air monitoring station. The measured laser irradiance data showed very little variation across the sessions and a single fitting equation was derived for the atmospheric scatter function. With very conservative estimates of the scatter from the human eye, atmospheric scatter was found to contribute no more than 5% to the overall veiling luminance across the scene for a human observer experiencing laser eye dazzle. It was concluded that atmospheric scatter does not make a significant contribution to laser eye dazzle for short-range laser engagements in atmospheres of good to moderate air quality, which account for 99.5% of conditions in San Antonio, Texas.

15. SUBJECT TERMS

16. SECURITY CLASSIFICATION OF: **Unclassified**			**17. LIMITATION OF ABSTRACT**	**18. NUMBER OF PAGES**	**19a. NAME OF RESPONSIBLE PERSON** Leon McLin
a. REPORT U	**b. ABSTRACT** U	**c. THIS PAGE** U	SAR Unclassified	8	**19b. TELEPHONE NUMBER** *(include area code)*

Research Article
Vol. 54, No. 25 / September 1 2015 / *Applied Optics* 7567

applied optics

Measuring the contribution of atmospheric scatter to laser eye dazzle

CRAIG A. WILLIAMSON,[1,2,*] J. MICHAEL RICKMAN,[3] DAVID A. FREEMAN,[4] MICHAEL A. MANKA,[3] AND LEON N. MCLIN[2]

[1]*Defence Science and Technology Laboratory, Dstl Porton Down, Salisbury, SP4 0JQ, UK*
[2]*711th Human Performance Wing, Human Effectiveness Directorate, Bioeffects Division, Optical Radiation Bioeffects Branch, 4141 Petroleum Rd, JBSA Fort Sam Houston, Texas 78234-2644, USA*
[3]*Engility, 4141 Petroleum Rd, JBSA Fort Sam Houston, Texas 78234-2644, USA*
[4]*NAMRU-SA, HJF, 4141 Petroleum Rd, JBSA Fort Sam Houston, Texas 78234-2644, USA*
**Corresponding author: cawilliamson@dstl.gov.uk*

Received 9 April 2015; revised 7 July 2015; accepted 15 July 2015; posted 16 July 2015 (Doc. ID 237791); published 25 August 2015

An experiment has been conducted to determine the contribution of atmospheric scatter to the severity of the dazzle experienced by a human under illumination from a visible laser. A 15 W 532 nm laser was propagated over a 380 m outdoor range in San Antonio, Texas, over nine data collection sessions spanning June and July 2014. A narrow acceptance angle detector was used to measure scattered laser radiation within the laser beam at different angles from its axis. Atmospheric conditions were logged via a local weather station, and air quality data were taken from a nearby continuous air monitoring station. The measured laser irradiance data showed very little variation across the sessions and a single fitting equation was derived for the atmospheric scatter function. With very conservative estimates of the scatter from the human eye, atmospheric scatter was found to contribute no more than 5% to the overall veiling luminance across the scene for a human observer experiencing laser eye dazzle. It was concluded that atmospheric scatter does not make a significant contribution to laser eye dazzle for short-range laser engagements in atmospheres of good to moderate air quality, which account for 99.5% of conditions in San Antonio, Texas.

OCIS codes: (010.1310) Atmospheric scattering; (140.7300) Visible lasers; (140.3360) Laser safety and eye protection; (290.5820) Scattering measurements; (330.4060) Vision modeling; (330.4595) Optical effects on vision.

http://dx.doi.org/10.1364/AO.54.007567

1. INTRODUCTION

Laser eye dazzle is the temporary visual obscuration caused by visible wavelength laser beams being incident upon the eye. Commercial airline pilots are regularly subjected to such dazzle through malicious laser use by individuals on the ground [1], while "laser dazzlers" are often used in military and security applications as nonlethal weapons with the aim of warning or determining intent [2].

Spatial variations in the refractive index of the ocular media serve to scatter light from intense light sources and spread their image across the visual field [3]. The subjective angular subtense of a laser source is determined by several factors, but primarily by the laser irradiance incident upon the eye (higher irradiance = larger dazzle field) and the ambient luminance (lower light level = larger dazzle field). Other contributing factors include the wavelength of the laser beam, and the age and pigmentation of the observer's eye [4].

In everyday outdoor conditions the above described "intraocular scatter" is not the only contributor to the severity of laser eye dazzle, as there are several extraocular (external to the eye) scattering components with the ability to influence the dazzle experience. Optical elements between the eye and the laser source, such as spectacles [5] or a windshield [6], are examples of extraocular scatter components which can affect the severity of laser eye dazzle.

This study concerns the contribution of another extraocular scatter source—the atmosphere through which the laser beam propagates. An intense laser beam can easily be viewed off axis (Fig. 1) because of atmospheric scattering. In this image light is scattered away from the axis of the laser and toward the viewer. When viewing the laser on axis, single or multiple atmospheric scattering processes can cause light to be directed toward the eye from angles outside of the laser axis, as shown schematically in Fig. 2. This light can add a "corona" of light around the central bright point source—a spatial spreading of the laser beam due to the eye receiving light from a wider angular subtense than it would have done in the absence of any atmospheric scattering.

Fig. 1. Laser beam viewed off axis.

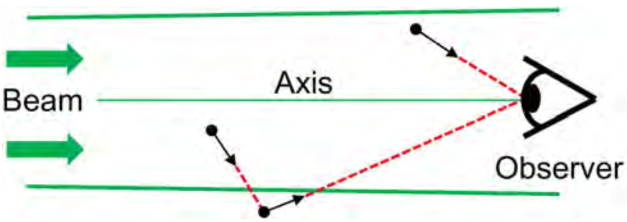

Fig. 2. Schematic of atmospheric scatter showing single and multiple scattering processes causing light to be directed toward the eye from angles outside of the laser axis.

Atmospheric scatter of visible wavelengths is primarily caused by fine particles (<2.5 μm diameter) suspended in the air which can diffract, refract, or phase shift light [7], and occurs predominantly in the forward direction (i.e., the direction in which the light is traveling). Such fine aerosols, typically originating from combustion processes, are more efficient at scattering and more plentiful in the atmosphere than coarse particles such as road dust and therefore dominate scattering processes. Air molecules are also capable of scattering but they are very inefficient at doing so and make a negligible contribution [7].

Atmospheric scatter and the resulting blur introduced to imaging systems has been well researched [8, 12], but there is a paucity of work in the literature looking at its impact on laser dazzle. The authors have recently developed a set of simple calculations to allow the visual impact of laser eye dazzle to be modeled [4]. The model outputs a minimum distance for visual detection of a target in the presence of laser dazzle, known as the nominal ocular dazzle distance (NODD). However, the initial version of the model only accounts for intraocular scatter and so the authors are seeking to incorporate the contributions of extraocular scatter to laser eye dazzle. Therefore, this experimental paradigm aims to understand the relative contribution of atmospheric scatter by comparison to the CIE general disability glare equation [13] and a modified version of this equation [4], both of which estimate the scatter within the eye.

2. METHOD

A. Principles

The experiments were designed to derive an equation for the angular distribution of atmospherically scattered laser radiation, sometimes referred to as a scatter or phase function. This scatter function describes the fraction of light scattered, per unit solid angle, in a given direction.

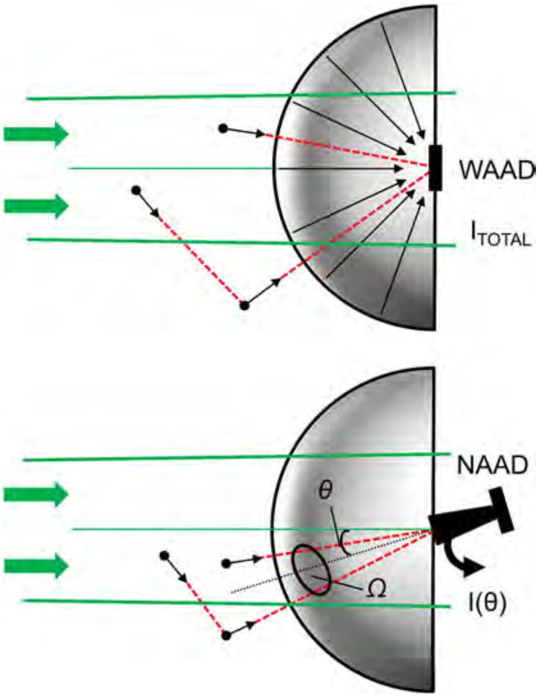

Fig. 3. Data collection schematic showing (top) wide acceptance angle detector (WAAD) and (bottom) narrow acceptance angle detector (NAAD).

Figure 3 shows a schematic of the experimental design. A laser was propagated over a distance and then a wide acceptance angle detector (WAAD), located on axis and normal to the laser path, was used to collect light from all angles and all directions in a hemisphere around the detector plane. The WAAD gathered both on axis and off axis forward scattered radiation from the laser source to provide a measure of the total irradiance, $I_{\mathrm{TOTAL}}(\mathrm{mW}\cdot\mathrm{cm}^{-2})$. A narrow acceptance angle detector (NAAD) was then used to sample around this hemisphere and measure the contribution, $I(\theta)(\mathrm{mW}\cdot\mathrm{cm}^{-2})$, to I_{TOTAL} within a fixed solid angle, Ω (sr), at a given angle, θ (deg), from the laser axis in a horizontal plane. The NAAD remained within the center of the laser beam but was rotated at varying angles, replicating the way an eye might rotate to view a scene when subjected to laser dazzle.

By gathering data at a range of angles, the atmospheric scatter function, $f(\theta)$ (sr^{-1}), can be expressed as the fraction of light scattered per unit solid angle:

$$f(\theta)=\frac{I(\theta)/\Omega}{I_{\mathrm{TOTAL}}}. \tag{1}$$

For a given laser irradiance at the eye, $U(\mathrm{W}\cdot\mathrm{m}^{-2})$, the resulting veiling luminance, $L_v(\mathrm{cd}\cdot\mathrm{m}^{-2})$, can then be calculated by the following relationship [14]:

$$L_V=f(\theta)\cdot 683\cdot V_\lambda\cdot U, \tag{2}$$

where V_λ is the eye's photopic efficiency at the laser wavelength, λ (0.885 for 532 nm), and 683 is the maximum photopic luminous efficacy in lumens per watt [15].

B. Implementation

The experiment was conducted at the Outdoor Directed Energy Site of the Tri Service Research Laboratory on Joint Base San Antonio Fort Sam Houston, Texas. This outdoor laboratory consists of a 400 m gravel track with a small building at one end (the “send” point) housing the laser, aligned with a 4 m high brick backstop at the other end (the “receive” point) where the measurement equipment was located inside an open trailer. The propagation distance from laser aperture to detector was measured as 380 m using both a rangefinder and a global positioning system receiver.

The laser source was a commercially available 532 nm laser system (Coherent Verdi V 18), chosen as its wavelength matched the most commonly used laser dazzle devices, while its higher power (~15 W) improved the ability to measure small amounts of scatter. The optical delivery system was designed to minimize system scatter by using a single broadband alignment mirror to direct the raw beam from the laser aperture toward the receive point (Fig. 4). During nonmeasurement procedures a second mirror, mounted to a motorized flipper mount, was inserted into the path to direct the laser output to a beam dump. With a divergence of around 0.3 mrad, center beam irradiances at the receive point were approximately $200\ \mathrm{mW} \cdot \mathrm{cm}^{-2}$.

The key measurement equipment located at the receive point was a detector system comprising two laser detectors (Thorlabs PDA100A) mounted on a two axis translation stage providing vertical and horizontal positioning (Fig. 5). The upper detector was the WAAD with a ±50° acceptance angle to give the I_{TOTAL} reading, under the assumption that the signal beyond this acceptance angle was negligible. The lower detector was the NAAD, with a designed 1° acceptance angle and actual value of 0.955° giving a solid angle, Ω, of 2.18×10^{-4} sr. The NAAD was mounted on a graduated rotation stage such that it could be positioned in azimuth independent of the upper detector.

The NAAD is pictured in Fig. 6 and consists of a 25.4 mm diameter, 60 mm focal length achromatic lens to focus incoming light through a precision 1 mm aperture in front of the detector. The effective input aperture diameter was 2.291 cm, which was the inner diameter of the retaining ring used to hold the lens in place. A summary of the NAAD dimensions is given in Table 1. The detector was mounted to the rotation stage with the lens positioned at the center of rotation.

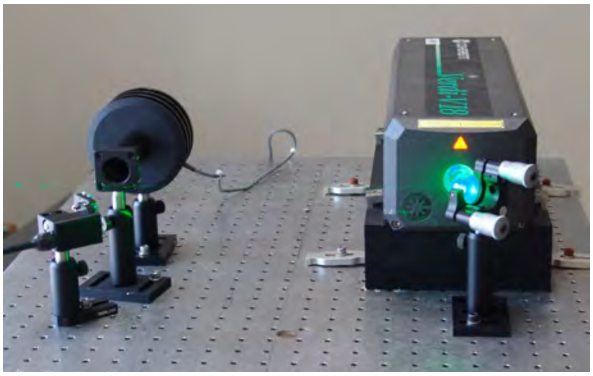

Fig. 4. Laser optical table setup.

Fig. 5. WAAD (top aperture) and NAAD (lower aperture) mounted on translation and rotation stages.

Fig. 6. Computer aided design drawing of the NAAD showing the lens (right), aperture (middle), and detector surface (left). The inset shows a drawing of the fully assembled NAAD.

Table 1. Dimensions and Calculations for the NAAD

Parameter	Value
Lens focal length (mm)	60
Detector aperture diameter (mm)	1
Calculated field of view (deg)	0.955
Calculated field of view (sr)	2.18×10^{-4}
Input aperture diameter (cm)	2.291
Input aperture area (cm^2)	4.122

As the assembly was rotated with respect to the direct incoming beam, the light focused by the lens translates off the aperture blocking it from reaching the detector. Only rays within the 1° acceptance angle reach the detector.

Both detectors were fitted with 532 nm laser line filters (Thorlabs FL532 3) to enhance their sensitivity by isolating the narrowband laser signal from the broadband ambient lighting. In their fully configured states, both detectors were calibrated for power measurements at each of their seven gain settings against a calibrated detector and optical power meter (Newport 918D and 2936 C). For the NAAD, the calculated total received power (W) was converted to irradiance (W · cm^{-2}) through division by the input aperture area as given in Table 1. For the WAAD the power was divided by the detector active area (0.754 cm^{2}) to give irradiance.

During each data point collection both detectors operated at their native 10 kHz rate over a period of 60 s to average out the effects of atmospheric turbulence. A LabVIEW software interface allowed the operators to obtain mean and standard deviation figures across the data collection period. The standard deviation as a percentage of the mean I_{TOTAL}, (StdDev%), was used as an approximate measure of the turbulence, under the assumption that other atmospheric processes did not vary during the data collection period.

Critical to the scatter measurement system was the inclusion of an obscuration disc in front of the NAAD, designed to block direct incident rays (see Fig. 7 and Fig. 8). While the direct beam was not within the field of view of the NAAD, the obscuration disc was necessary to prevent the high power direct beam from entering the lens of the NAAD from where internal reflections could potentially reach the detector surface. The size of the disc was slightly larger than the NAAD aperture at approximately 25 mm, which facilitated alignment by casting a shadow across the NAAD aperture. The obscuration disc had to be located greater than 2.51 m away from the NAAD aperture to ensure that it did not encroach upon that detector's field of view and block any scattered light that was part of the desired measurement.

Also used in the setup was a camera (Cohu 4815) to profile the beam prior to each experiment. The camera also aided in aligning the detectors to the center of the beam via the translation stages, as can be seen in Fig. 9.

To record atmospheric conditions during the experiments, a wireless weather station (Davis Vantage Pro2 Plus) was located at the test site. Captured data of relevance included temperature, humidity, atmospheric pressure, and solar radiation. For atmospheric quality, the concentration of particles less than 2.5 µm diameter (PM 2.5 in units of $\mu\text{g} \cdot \text{m}^{-3}$) was recorded based upon data published by the Texas Commission on Environmental Quality from a continuous air monitoring station (CAMS) located approximately four miles south of the test site (City Public Service Energy CAMS 678) [16]. As a secondary measure of air quality the meteorological visibility was recorded from weather data at San Antonio International Airport [17], which is located approximately five miles north west of the test site.

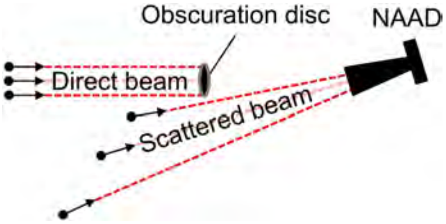

Fig. 7. Illustration of the obscuration disc used to block the direct beam from entering the NAAD optics.

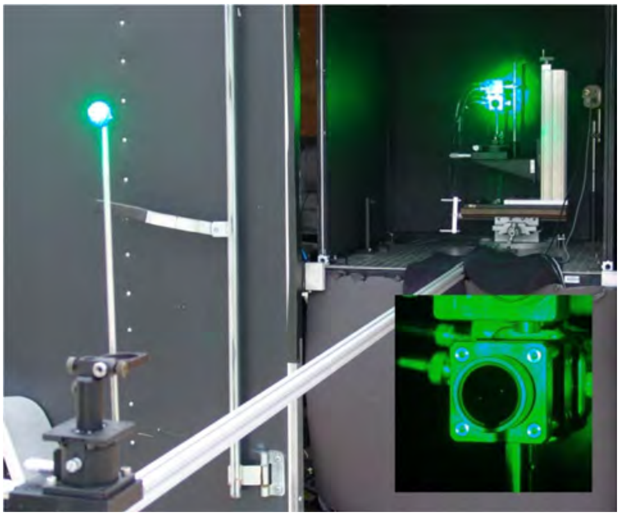

Fig. 8. Obscuration disc on the left mounted on a thin pole, casting a shadow across the aperture of the NAAD on the right (close up lower right).

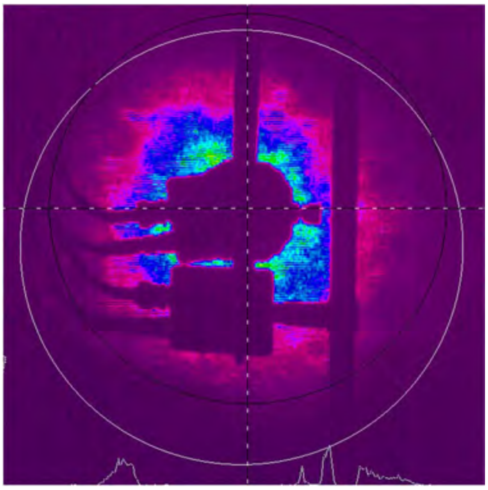

Fig. 9. Beam profile image used for detector alignment.

C. Procedure

The laser was first directed to be roughly incident upon the detectors by adjustment of the laser output alignment mirror at the send point, facilitated by radio communications with the receive point. The detector system's translation stage was then moved to bring the WAAD detector into the center of the beam while viewing the image from the beam profile camera and maximizing the received laser irradiance reported from the detector.

To ensure that the WAAD detector surface was normal to the laser beam, a small aperture was temporarily placed approximately 1 m in front of the detector and the detector was adjusted so the backreflection from the detector surface showed as a bright spot on the rear of the aperture. The alignment of the detector was then fine tuned to ensure that the reflected beam traveled perfectly back through the aperture, thus indicating normal alignment with the laser beam.

Before each measurement commenced, the detector was zeroed by blocking the beam at the source and initiating a zeroing routine in the software to remove ambient light from the readings. After unblocking the laser, a 60 s data collection period was initiated to derive the initial value for I_{TOTAL} (typically around 200 $\mathrm{mW \cdot cm^{-2}}$, as previously noted).

The NAAD was then centered in the beam with the translation stage and set to be normal to the laser beam using the same alignment method as used previously. It was then rotated about its center axis to a starting angle of 1° and the obscuration disc was placed at the predetermined distance of greater than 2.51 m from the detector. The obscuration disc was first aligned by eye to ensure that its shadow completely covered the NAAD's aperture, and then alignment was fine tuned by minimizing the measured irradiance on the detector. The starting angle of 1° ensured that the obscuration disc was not within the detector's field of view, and also that the Arago spot (the bright spot at the center of the disc's shadow caused by Fresnel diffraction) had no measurable impact on the detector.

At this point the NAAD irradiance was zeroed and the 60 s data collection began to capture the value for $I(1°)$, which was typically around 200 $\mathrm{nW \cdot cm^{-2}}$. The detector was subsequently rotated by 0.5°, following which the obscuration disc alignment was fine tuned, the NAAD was zeroed once more and data gathering began again. This procedure was repeated until the signal detected by the NAAD reached its sensitivity floor of approximately 1 $\mathrm{nW \cdot cm^{-2}}$, which generally occurred around 10° from the laser axis. To verify that the small signals at large angles were from the laser, and not noise, a chopper wheel was used at the laser output aperture to encode a 100 Hz signal on the beam. Viewing the received irradiance in the frequency domain showed a clear peak at the chopping frequency, thus verifying that the signal was indeed from the laser source.

Finally, the NAAD was moved back to 1° and another measurement taken in order to ensure consistency across the data collection period, which typically took around 1 h. The WAAD detector was then moved back into the center of the beam and another value for I_{TOTAL} measured, which was subsequently averaged with the initial measurement to give the final value. As can be seen from Fig. 9 the beam size was not large enough to permit continuous monitoring of I_{TOTAL} throughout the experiment, and so the averaging of start and end readings provides some compensation for any changes in beam quality, turbulence, or atmospheric transmission across the test period.

With I_{TOTAL} and all $I(\theta)$ data collected, the scatter values, $f(\theta)$, could then be calculated using Eq. (1).

3. RESULTS AND DISCUSSION

Data were collected on nine separate sessions across June and July 2014. A summary of the atmospheric conditions for these dates is given in Table 2. Atmospheric parameters were averaged over the data collection periods (approximately 1 h each) wherever possible, or taken from time periods in the middle of the collection period.

Testing spanned dates with good (PM 2.5 less than 12 $\mathrm{\mu g \cdot m^{-3}}$) and moderate (between 12 and 35 $\mathrm{\mu g \cdot m^{-3}}$) air quality [16], with temperatures ranging from 68°F to 95°F and humidity ranging from 51% to 93%. Two data sessions took place at night with no measurable solar radiation, while the others took place during the morning or peak afternoon sunshine. The StdDev% factor, giving a rough indication of turbulence from the standard deviation of the mean I_{TOTAL}, ranged from 12% (low turbulence) up to 75% (high turbulence). The visibility data from the airport location usually followed the trend of the PM 2.5 data, with concentrations of more than 14 $\mathrm{\mu g \cdot m^{-3}}$ corresponding with visibility less than 10 miles. The one exception was data for 09 July, which indicated the highest recorded PM 2.5 concentration but a visibility of greater than 10 miles. This could be due to the separation of the airport from the CAMS by approximately 8.5 miles, with the possibility of localized weather conditions.

An aggregated scatter graph across all nine data collection periods is shown in Fig. 10. It can be seen that the atmospheric scatter data were very similar for each collection period, with the ±1 standard deviation error bars (not shown on this graph for clarity) for each collection period mostly encompassing each other. There are some outliers in the dataset, most notably the

Table 2. Summary of Atmospheric Conditions for the Nine Days of Data Collection

Date	Time	Solar ($\mathrm{W \cdot m^{-2}}$)	Temp. (°F)	Humidity (%)	Pressure (mb)	PM-2.5 ($\mu\mathrm{g \cdot m^{-3}}$)	Visibility (miles)	StdDev% (%)
04 June	09:00	338	78	81	1011.3	6.3	>10	38
05 June	09:00	280	79	79	1009.1	9.4	>10	30
06 June	09:00	374	80	77	1011.2	25.3	9	60
09 June	09:00	133	78	81	1007.1	14.4	8	21
10 June	05:00	<1	68	93	1008.9	7.5	>10	12
12 June	15:00	780	95	51	1007.2	13.4	>10	75
24 June	10:00	454	83	75	1015.0	11.1	>10	61
07 July	09:30	537	81	67	1014.9	25.4	8	69
09 July	04:30	<1	75	86	1014.7	25.9	>10	17

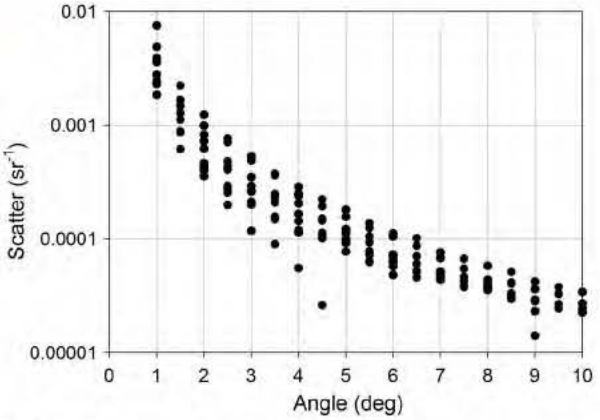

Fig. 10. Scatter versus angle from all nine data collection sessions.

lowest set of data points at 2.5° to 4.5° that were all from 04 June. While the PM 2.5 for that day was the lowest of the nine sessions, it was only marginally better than other days and there were no other noticeable differences in the atmospheric conditions for that day. The dissimilarity with the subsequent eight data sessions leads the authors to believe that an experimental error may have occurred during the data collection possibly an unintentional movement of the detector beyond the angle displayed on its rotation stage. Data from 04 June were therefore removed from the dataset for the subsequent analysis.

Fig. 11 shows a plot of the highest (09 July) and lowest (24 June) recorded scatter functions from the reduced set of eight data collections sessions, with error bars indicating ±1 standard deviation. The short error bars for 09 July indicate low turbulence (StdDev% = 17%) compared with the large error bars for 24 June (StdDev% = 61%). Within the measured errors, both scatter functions are very close. Looking at the summary weather statistics it could be argued that any scatter differences are due to the high PM 2.5 concentration on 09 July (25.9 $\mu g \cdot m^{-3}$) compared with 24 June (11.1 $\mu g \cdot m^{-3}$). However, Fig. 12 shows a comparison of the scatter functions recorded for another set of high (07 July, 25.4 $\mu g \cdot m^{-3}$) and low (10 June, 7.5 $\mu g \cdot m^{-3}$) PM 2.5 values where there is no noticeable difference in the scatter functions.

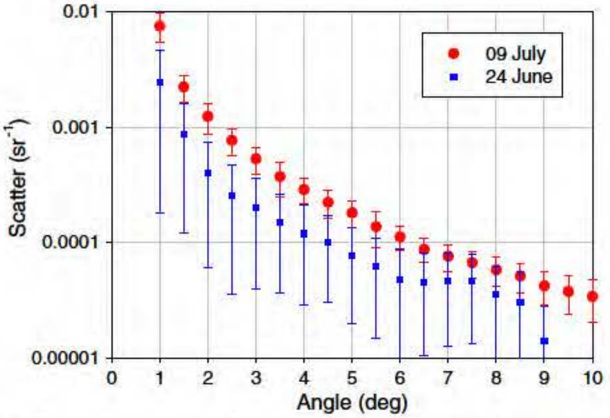

Fig. 11. Comparison of highest and lowest scatter captured.

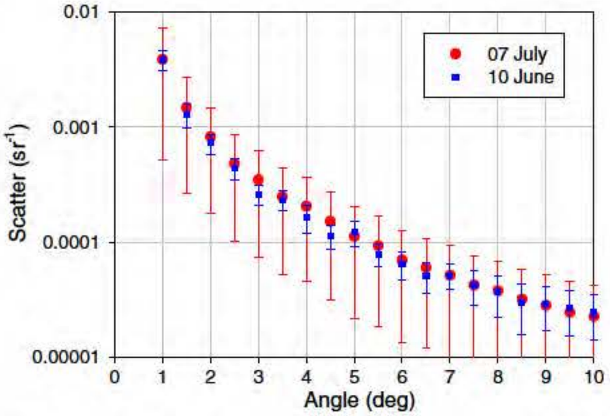

Fig. 12. Comparison of scatter for highest and lowest PM 2.5 concentrations.

Fig. 13 shows a comparison of scatter data from 10 June and 12 June: the days of lowest and highest solar radiation (<1 versus 780 $W \cdot m^{-2}$), lowest and highest temperature (68°F versus 95°F), highest and lowest humidity (93% versus 51%), and lowest and highest StdDev% turbulence (12% versus 75%). The higher turbulence accompanies the high temperature, high solar radiation condition to give much larger uncertainties for the 12 June data, but the mean values look broadly similar to 10 June. The similarity given the vastly different solar radiation levels (dark night versus peak summer day) shows that the experimental implementation and procedure were robust to influence from ambient light. It also indicates that the measures taken to average out turbulence effects were successful. In terms of scatter dependencies, the data suggest that temperature and humidity do not affect atmospheric scattering, at least across the range of values that these two datasets represent and when averaged over 60 seconds.

Fig. 14 shows all mean data from the reduced set of eight collection sessions, together with the following line of best fit scatter function ($R^2 = 0.95$):

$$f(\theta) = 0.0031\,\theta^{-2.095}. \tag{3}$$

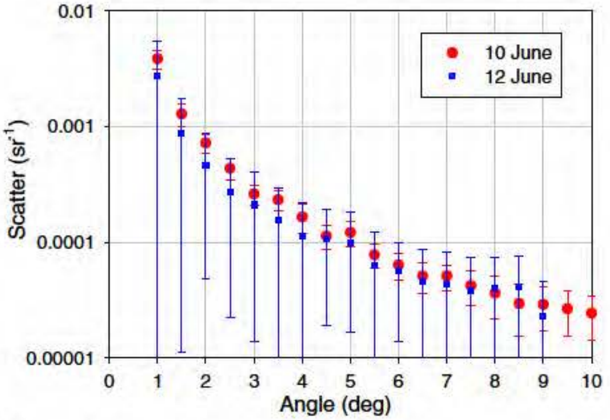

Fig. 13. Comparison of scatter for highest and lowest solar radiation and temperature.

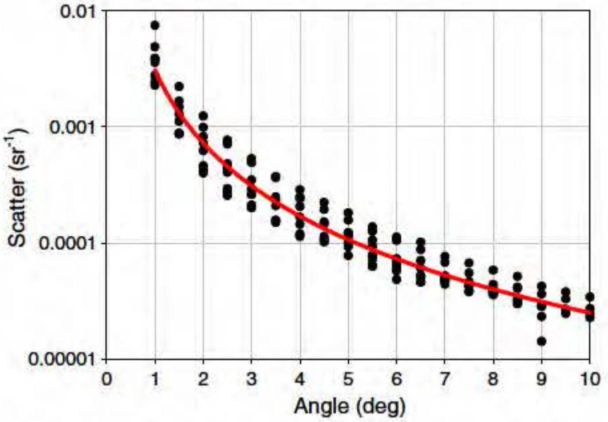

Fig. 14. All data from reduced set of eight data collection sessions together with line of best fit.

In Fig. 15, this scatter function is compared with the glare due to scatter in the human eye in order to understand the overall contribution of atmospheric scatter to laser eye dazzle. The upper curve is generated from the CIE general disability glare equation an internationally accepted standard equation for intraocular scatter, based upon human subject measurements [13]. The CIE equation accounts for increasing scatter with age and lighter eyes, and so the plotted graph is for the lowest possible scatter case of a 20 year old with very dark eyes. It can be seen that scatter from the eye, even in this lowest scatter case, is still over 3 orders of magnitude greater than the scatter from the atmosphere found in the present experiment.

The authors have previously presented an adjustment to the CIE general disability glare equation which suggests a lower scatter in low ambient luminance levels when simulating laser exposures [4,18]. Using this adjustment factor with a night time ambient luminance level of 0.001 cd · m^{-2} gives the middle dotted line in Fig. 15. This now represents the lowest possible predicted intraocular scatter, based on a 20 year old with dark eyes viewing in the lowest ambient lighting conditions. Even in this case, the predicted atmospheric scatter is less than 5% of the predicted eye scatter.

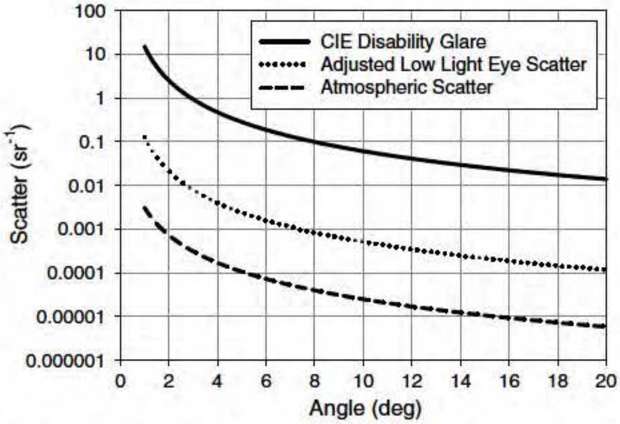

Fig. 15. Comparison of the atmospheric scatter measured in this experiment to the predicted eye scatter from the CIE general disability glare equation, and a version adjusted for low ambient light level laser exposures.

Referring back to Eq. (2), each scatter function can be used to estimate an equivalent veiling luminance distribution on the retina. Taking a 532 nm laser exposure of 500 μW · cm^{-2} (half the maximum permissible exposure for a 10 s visible wavelength exposure, based upon laser safety standards [19]), and an angle from the laser axis of 5°, gives an equivalent veiling luminance caused by the atmospheric scatter of 0.3 cd · m^{-2}. This compares with 7 cd · m^{-2} caused by the adjusted low light eye scatter case, and 852 cd · m^{-2} by the CIE case. The veiling luminance equation, Eq. (2), maintains the relative magnitude of the atmospheric contribution, with it being less than 5% of the luminance caused by the adjusted eye equation and less than 0.05% of the luminance of the CIE eye equation.

4. CONCLUSIONS

The results generated by this study suggest that a robust experiment has been devised for the measurement of atmospheric scatter. It has been demonstrated that very small levels of atmospheric scatter (~nW · cm^{-2}) can be measured, independent of ambient light level and atmospheric turbulence.

For short range laser engagements in atmospheres of good to moderate air quality, this study suggests that atmospheric scatter has a negligible impact upon laser eye dazzle. Even with very conservative estimates of the scatter contribution from the human eye, the atmospheric scatter adds no more than 5% to the overall scatter for a laser propagating over a distance of 380 m. Such scatter levels would not create any significant additional veiling luminance across the scene for a human observer when compared to the veiling luminance introduced by the scatter within the eye.

The magnitude of atmospheric scatter does not show any clear correlation with atmospheric quality based on PM 2.5 concentrations, at least for the good and moderate PM 2.5 levels experienced across the 380 m range. Higher PM 2.5 concentrations could cause an increase in the significance of atmospheric scatter, although the present experiment cannot further inform such predictions.

A statistical study of historical PM 2.5 data from the CAMS 678 site [16] shows that, from 2011 to 2013, there has only been an average of 43 hours per year where the PM 2.5 concentration has risen above 35 μg · m^{-3} and into the "unhealthy" category. This generally occurs in very narrow time periods, on average for 3 hours out of 14 days per year. Therefore, the results presented herein can be applied 99.5% of the time during an average year at the test site. To explore PM 2.5 scatter dependencies further would require relocation of the experiment to an environment with much poorer air quality than generally experienced in San Antonio. Alternatively, the use of artificial, localized atmospheric disturbances (e.g., smoke) could be considered.

It is anticipated that longer propagation ranges would increase the significance of atmospheric scatter, due to the greater volume of atmosphere for light interaction. Again, the present experiment cannot directly inform such predictions, but the relocation of the experiment to a longer range would provide additional data for comparison. The use of large mirrors at the receive point of the current test site, to reflect the beam and double the path length, is another option.

Within the environmental parameters encompassed by this experiment, atmospheric scatter appeared to be independent of temperature, humidity, and atmospheric pressure given equivalent PM 2.5 concentrations. However, the collection of additional data during, for example, very cold conditions would provide a useful comparison to further confirm this finding.

Additional improvements are possible to better understand how air quality influences this measurement. Having the capability to measure air quality at the test site would be preferable to account for any localized variations, and this would also allow artificial pollutants to be used and monitored. Use of a scintillometer to measure the refractive index structure parameter, C_n^2, would be beneficial to characterize turbulence. Using a higher power laser would also provide additional signal for measurements, potentially allowing data collection beyond the 10° limit found with the 15 W laser.

Finally, a natural extension to this experimental work would be the introduction of a theoretical component. Previously reported models [8 12] could be validated with the experimental data, and attempts made to apply the simulations to longer ranges and higher PM 2.5 concentrations.

Funding. Dstl; USAF.

Acknowledgment. The views expressed in this paper are those of the authors and do not necessarily reflect the official policy or position of the Department of the Navy, Department of Defense, nor the U.S. Government. The Navy's work was supported by work unit number G1401. This work was prepared as part of the authors' official duties. Title 17 U.S.C. Section 105 provides that "Copyright protection under this title is not available for any work of the United States Government." Title 17 U.S.C. Section 101 defines a U.S. Government work as a work prepared by a military service member or employee of the U.S. Government as part of that person's official duties.

REFERENCES

1. Aero News Network, "FAA: laser incidents increase in 2013," February 2014, http://www.aero-news.net/index.cfm?do=main.textpost&id=8f22d466-82d3-47bb-ab52-c2d92975093e.
2. Joint Non Lethal Weapons Program, "Non lethal optical distracters fact sheet," October 2011, http://jnlwp.defense.gov/Portals/50/Documents/Press Room/Fact Sheets/NLOD Fact Sheet Oct 2011.pdf.
3. D. P. Pinero, D. Ortiz, and J. L. Alio, "Ocular scattering," Optom. Vis. Sci. **87**, E682–E696 (2010).
4. C. A. Williamson and L. N. McLin, "Nominal ocular dazzle distance (NODD)," Appl. Opt. **54**, 1564–1572 (2015).
5. G. C. De Wit and J. E. Coppens, "Stray light of spectacle lenses compared with stray light in the eye," Optom. Vis. Sci. **80**, 395–400 (2003).
6. P. Padmos, "Glare and tunnel entrance lighting: effects of stray light from eye, atmosphere and windscreen," CIE J. **3**, 1–24 (1984).
7. W. C. Malm, *Introduction to Visibility* (Colorado State University, 1999).
8. L. R. Bissonnette, "Imaging through fog and rain," Opt. Eng. **31**, 1045–1052 (1992).
9. B. BenDor, A. D. Devir, G. Shaviv, P. Bruscaglioni, P. Donelli, and A. Ismaelli, "Atmospheric scattering effect on spatial resolution of imaging systems," J. Opt. Soc. Am. A **14**, 1329–1337 (1997).
10. N. S. Kopeika, "Aerosol modulation transfer function: An overview," in *Conference on Propagation and Imaging through the Atmosphere*, L. R. Bissonnette and C. Dainty, eds. (1997), pp. 214 225.
11. N. S. Kopeika, L. Dror, and D. Sadot, "Causes of atmospheric blur: comment on atmospheric scattering effect on spatial resolution of imaging systems," J. Opt. Soc. Am. A **15**, 3097–3106 (1998).
12. T. Carmon, L. Langof, U. Oppenheim, and A. D. Devir, "Atmospheric PSF caused by light scattering, comparison of a Monte Carlo model to experimental results," Proc. SPIE **3763**, 199–207 (1999).
13. J. Vos, B. Cole, H. W. Bodmann, E. Colombo, T. Takeuchi, and T. J. T. P. van den Berg, "CIE equations for disability glare," CIE TC Report CIE 146:2002 (2002).
14. J. Vos, "Disability glare a state of the art report," CIE J. **3**, 39–53 (1984).
15. G. Wyszecki and W. S. Stiles, *Color Science, Concepts and Methods, Quantitative Data and Formulae*, 2nd ed. (Wiley, 1982).
16. Texas Commission on Environmental Quality, CPS Pecan Valley CAMS 678, http://www.tceq.state.tx.us/cgi-bin/compliance/monops/daily summary.pl and http://www.tceq.state.tx.us/cgi bin/compliance/monops/yearly summary.pl.
17. National Weather Service, Weather Observations for San Antonio International Airport, http://w1.weather.gov/data/obhistory/KSAT.html.
18. L. N. McLin, P. A. Smith, L. E. Barnes, J. R. Dykes, T. Kuyk, B. J. Novar, P. V. Garcia, and C. A. Williamson, "Scaling laser disability glare functions with 'k' factors to predict dazzle," presented at ILSC 2013 International Laser Safety Conference, Orlando, USA, 18 21 March 2013.
19. American National Standards Institute, "American national standard for safe use of lasers," ANSI Z136.1 2014 (American National Standards Institute, 2014).